International Journal of Fluid Power 9 (2008) No. 2 pp. 15-25

LEAKAGE FAULT DETECTION IN HYDRAULIC ACTUATORS SUBJECT TO UNKNOWN EXTERNAL LOADING

Liang An and Nariman Sepehri

Department of Mechanical and Manufacturing Engineering, The University of Manitoba, Winnipeg, MB, Canada R3T 5V6
nariman@cc.umanitoba.ca

Abstract

This paper describes development and experimental evaluation of a hydraulic actuator leakage fault detector based on the extended Kalman filtering (EKF). Identification of external leakage at either side of the actuator as well as the internal leakage between the two chambers is examined. The present work is built upon previous work by the authors, but incorporates a significant improvement in that the new scheme is capable of detecting leakage faults for actuators that are also subject to unknown loading and/or significant friction. Experiments on a laboratory-based hydraulic actuator, using both structured (sinusoidal) and unstructured (pseudorandom) test signals show that: (*i*) under normal (no-fault) operating condition, the EKF-based state estimator closely predicts the states of the system and the external load, including actuator friction, using only a few measurements, (*ii*) in the presence of leakage faults, the level of residual errors between the estimated and the measured line pressures increase indicating the occurrence of faults and (*iii*), different leakage fault types and levels can be identified by tracking the pattern of the residual errors and without a need to model leakage faults. The present work lays a foundation for developing on-line leakage monitoring systems for hydraulic actuators.

Keywords: fault detection and isolation, extended kalman filtering, leakage, hydraulic actuators, friction, environmental interaction.

1 Introduction

Fluid powered systems are used in many applications including aircraft and off-highway machines. Reliability is crucial for proper operation in these applications. Thus, investigation into improved control and enhanced reliability in fluid power systems is of great importance to both academic and industrial fields. The general objective of the research, of which this paper forms a part, is to develop effective fault diagnosis schemes that can report abnormal operating conditions and locate various faults that can degrade the performance of hydraulic actuators.

Faults in hydraulic systems cover a wide range, from component failure and fluid contamination to pipe leakage and material wear (Zavarehi et al., 1999; Zhou et al., 2002; Khan et al., 2005). However, one of the greatest concerns is the leakage of hydraulic fluid. Besides deteriorating the performance, leakage can cause environmental damage – prompt identification of this fault is of industrial concern. Leakage in cylinders can be classified into either internal or external. If the fluid leaks within the hydraulic circuit, it is called internal leakage. If the fluid leaks outside or collected by the reservoir, it is considered external. One main cause of internal leakage is the wear in moving components (Skormin and Apone, 1995). Mechanically, a tiny leakage is designed between the moving parts to guarantee non-stick movements without excessive friction and to supply necessary lubrication for the contact surface. Contamination, including tiny particles of metal and sealing materials caused by wear, can gradually deteriorate this condition by widening the clearance between the moving parts and eventually cause the performance of the system to fall out of the designed tolerance. Component defects and poor connections are causes that contribute to external leakage in a hydraulic cylinder.

Research on fault detection and isolation (FDI) schemes applied to hydraulic systems were built upon many methods including recursive least squares algorithms (Skormin et al., 1994; 1995), artificial neural networks (Crowther et al., 1998; Le et al., 1998) and observer-based schemes (Khan et al., 2005; Frank, 1994). The successful application of extended Kalman filtering (EKF) towards fluid power fault diagnosis has also been reported in many research articles. Zavarehi et al. (1999)

This manuscript was received on 13 January 2008 and was accepted after revision for publication on 16 June 2008

showed the feasibility of applying an EKF algorithm on modeling a two-stage proportional servovalve. They showed that it is possible to monitor key parameters of the servovalve, such as discharge coefficient or friction parameters between the valve spool and its housing. Zhang and Jiang (2002) developed an active fault-tolerant control scheme for a class of hydraulic actuators used in aircraft for which an adaptive Kalman filter was employed to detect parameter changes due to faulty conditions. Chinniah et al. (2003) developed an EKF-based method to estimate actuator viscous friction as well as the effective bulk modulus. An and Sepehri (2003) studied the feasibility of an EKF-based FDI scheme in a hydraulic actuator with incorrect supply pressure. The scheme was later extended to detect actuator internal and external leakage faults (An and Sepehri, 2005). A model of dry friction having known parameters was integrated, for the first time, in the EKF estimator. Accurate modeling of friction, however, is difficult and friction parameters are subject to change over time. Thus, precise measurement of friction parameters to be used in the model for each individual actuator is a difficult task, if not impossible. Additionally, the actuation system was only considered in an unloaded mode and under structured reference signals. In actual applications, hydraulic actuators must respond to various reference signals while inevitably experience loading conditions. Examples are positioning of an aircraft control surface or motion control of an excavator boom.

In this paper, we extend the earlier work to include both friction and loading as unknown external disturbances. We verify experimentally the feasibility of applying an EKF-based state estimation approach for identification of actuator leakage types and levels in nonlinear electro-hydraulic systems and in presence of unknown external loading, significant actuator friction as well as pseudorandom reference input signals. The leakage faults include external leakage on either side of the actuator cylinder and internal (cross-port) leakage between the two cylinder chambers. The goal is to contribute to the development of on-line health monitoring of hydraulic actuators.

2 Description of the Test Rig

A picture of the hydraulic actuator upon which all tests are conducted is shown in Fig. 1. Powered by a motor-driven hydraulic pump, the actuation system operates with the fluid pressure of 13.8 MPa. The movement of the actuator (with a 610 mm stroke) is controlled by a Moog D765 servovalve with the flow capacity of 34 L/min at 21 MPa supply pressure. The valve accepts analog command signals from a high-speed PC equipped with a data acquisition board. A force sensor (0 ~ 22000 N) is mounted at the end of the rod to measure the environmental resistance produced by a spring that can generate 6000 N when being compressed by 1 cm. The displacement of the actuator is obtained by a rotary optical encoder via a Metrabyte M5312 quadrature incremental encoder card and the chamber pressures are measured by sensors located at each side of the cylinder.

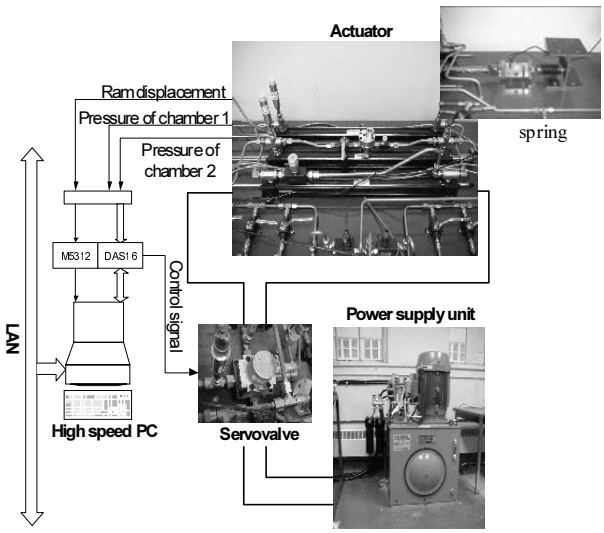

Fig. 1: *Hydraulic test station on which all experiments were performed; external load is emulated by a spring*

Figure 2 shows the schematic of the test rig. The manner in which leakage fault is produced is also shown in this figure. With reference to Fig. 2, the internal leakage is produced by bypassing fluid across the piston. This is achieved by connecting the two chambers of the actuator and controlling the flow by an adjustable needle valve (see a similar approach by Crowther et al., 1998). The internal leakage flow rate q_{il} is measured using a positive displacement flowmeter (JVA-KL series by AW Company) with a 7.6 L/min range and accuracy of ± 0.5 %. To produce the external leakage, a portion of the fluid flow from either side of the actuator is bypassed to the reservoir by opening the corresponding needle valves. External leakage flows, q_{el1} and q_{el2}, are measured using positive-displacement flowmeters.

3 Development of the Scheme

In this section the model of the hydraulic actuator under a normal operating condition is described first. This model is then used within an extended Kalman filter to predict selected states for both normal and faulty conditions. Note that in the development of the leakage fault detector, no model of the leakage is included and leakage levels are not explicitly estimated.

3.1 System Model

Using a linear orifice area gradient, w, the spool displacement, x_{sp}, is related to the servovalve flows, q_1 and q_2, as shown below (Merritt, 1967):

$$\begin{cases} q_1 = C_d w x_{sp} \sqrt{\dfrac{2}{\rho}(p_s - p_1)} \\ q_2 = C_d w x_{sp} \sqrt{\dfrac{2}{\rho}(p_2)} \end{cases} \quad x_{sp} \geq 0 \qquad (1)$$

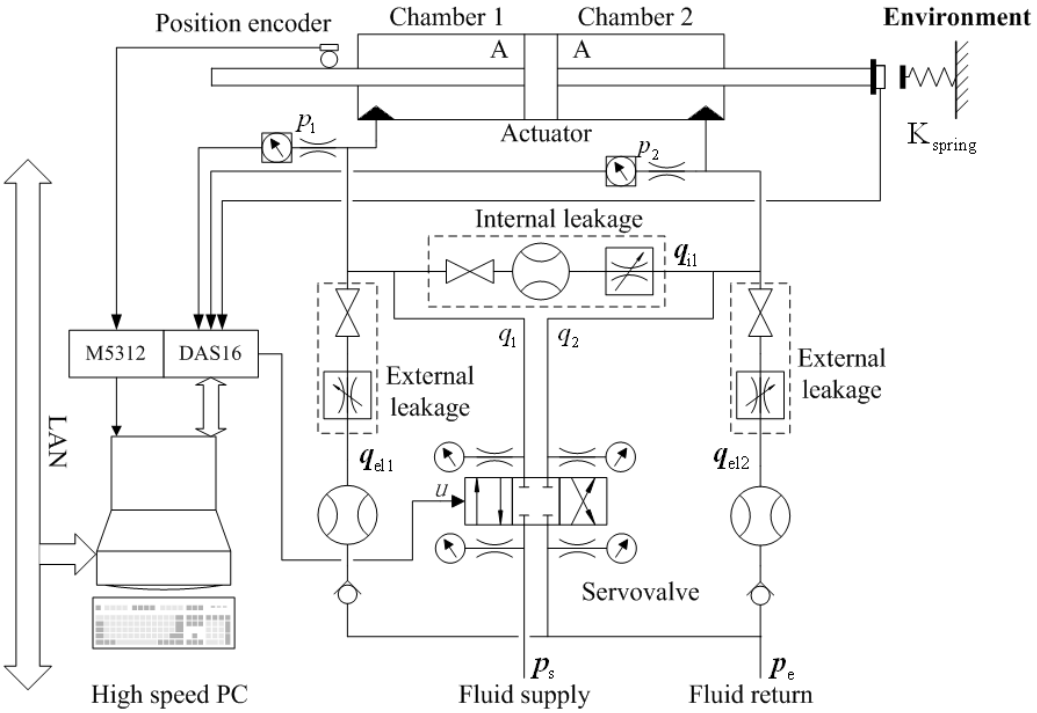

Fig. 2: *Schematic of test station. Internal and external leakage fault producing components are enclosed in dashed lines*

$$\begin{cases} q_1 = C_d w x_{sp}\sqrt{\dfrac{2}{\rho}(p_1)} \\ q_2 = C_d w x_{sp}\sqrt{\dfrac{2}{\rho}(p_s - p_2)} \end{cases} \quad x_{sp} < 0 \tag{2}$$

C_d is the orifice coefficient of discharge, and ρ represents the density of the hydraulic oil. Pressure and flow variables are shown in Fig. 1. Continuity equations for the hydraulic flows between the servovalve and the actuator are given by the following relations:

$$\begin{cases} q_1 = A\dot{x}_a + \dfrac{1}{\beta}V_1(x_a)\dot{p}_1 \\ q_2 = A\dot{x}_a - \dfrac{1}{\beta}V_2(x_a)\dot{p}_2 \end{cases} \tag{3}$$

x_a represents the actuator displacement and β is the effective bulk modulus of the hydraulic fluid. Note that Eq. 3 represents the normal operating (no leak) condition. $V_1(x_a)$ and $V_2(x_a)$ are the volumes of the fluid trapped in either chambers of the actuator and expressed by the following equations:

$$\begin{cases} V_1(x_a) = V_1^0 + A(x_a - X_{min}) \\ V_2(x_a) = V_2^0 + A(X_{max} - x_a) \end{cases} \tag{4}$$

where V_1^0 and V_2^0 are the volumes of hydraulic fluid in the corresponding supply pipes. X_{min} and X_{max} are positions of the piston in its fully-retracted and fully-extended positions, respectively. The dynamic relation between the servovalve input signal, u, and the spool displacement, x_{sp}, is expressed by a second-order differential equation:

$$u = \frac{1}{k_{sp}\omega_n^2}\ddot{x}_{sp} + \frac{2d_m}{k_{sp}\omega_n}\dot{x}_{sp} + \frac{1}{k_{sp}}x_{sp} \tag{5}$$

Parameter ω_n is the natural frequency, k_{sp} is the gain, and d_m is the effective damping ratio.

When working, the actuator interacts with the environment and experiences loading. Also, the actuator exhibits substantial friction that could change with time. Thus, the effect of loading as well as friction must be included in the model:

$$(P_1 - P_2)A = m\ddot{x}_a + F_e \tag{6}$$

The left-hand side of Eq. 6 is the actuation force generated by pressure differential ($P_1 - P_2$). In Eq. 6, actuator friction has been considered unknown and has been lumped together with the external loading originated from the environment. It is represented as F_e.

3.2 EKF Estimator

The model described by Eq. 1 to 6, represents the hydraulic actuator system under the normal operating condition. From the EKF view point, it can be regarded as a stochastic process with process noise $\boldsymbol{w}$ and measurement noise $\boldsymbol{v}$:

$$\begin{cases} \dot{\boldsymbol{x}} = \mathbf{f}(\boldsymbol{x}, u) + \boldsymbol{w} \\ \boldsymbol{y} = \mathbf{h}(\boldsymbol{x}) + \boldsymbol{v} \end{cases} \tag{7}$$

where u is the input signal, $\boldsymbol{x}$ is the vector of states, and $\boldsymbol{y}$ is the vector of measured outputs. Considering the external resistance F_e in Eq. 6 as unknown, the following state space model is derived from Eq. 1 to 6:

$$\begin{cases} \dot{x}_1 = x_6 + w_1 \\ \dot{x}_2 = \begin{cases} \dfrac{\beta}{V_i(x_4)}[C_d w x_1\sqrt{\dfrac{2}{\rho}(p_s - x_2)} - Ax_5] + w_2 & x_1 > 0 \\ \dfrac{\beta}{V_i(x_4)}[C_d w x_1\sqrt{\dfrac{2}{\rho}(x_2)} - Ax_5] + w_2 & x_1 \le 0 \end{cases} \\ \dot{x}_3 = \begin{cases} \dfrac{\beta}{V_o(x_4)}[-C_d w x_1\sqrt{\dfrac{2}{\rho}(x_3)} + Ax_5] + w_3 & x_1 > 0 \\ \dfrac{\beta}{V_o(x_4)}[-C_d w x_1\sqrt{\dfrac{2}{\rho}(p_s - x_3)} + Ax_5] + w_3 & x_1 \le 0 \end{cases} \\ \dot{x}_4 = x_5 + w_4 \\ \dot{x}_5 = \dfrac{1}{m}(Ax_2 - Ax_3 - F_e) + w_5 \\ \dot{x}_6 = -2d_m\omega_n x_6 - \omega_n^2 x_1 + k_{sp}\omega_n^2 u + w_6 \\ \dot{x}_7 = w_7 \end{cases} \tag{8}$$

where $\boldsymbol{x} = [x_{sp}, p_1, p_2, x, \dot{x}, x_{sp}, F_e]^T$. Note that the unknown disturbance, F_e, is characterized as a stochastic process that has impact on the actuator. Consequently it can be modeled as a random signal with certain mean that is deteriorated by noise with certain density. As will be seen later, this approach produces results that are reasonably justified. The state space model (Eq. 8) is now discretized, using the forward difference method:

$$\begin{cases} x_1(k+1) = Tx_6(k) + x_1(k) + w_1(k) \\ x_2(k+1) = \begin{cases} \dfrac{T\beta}{V_1(x_4(k))}[C_d w x_1(k)\sqrt{\dfrac{2}{\rho}(p_s - x_2(k))} \\ -Ax_5(k)] + x_2(k) + w_2(k) & x_1(k) > 0 \\ \dfrac{T\beta}{V_1(x_4(k))}[C_d w x_1(k)\sqrt{\dfrac{2}{\rho}(x_2(k))} \\ -Ax_5(k)] + x_2(k) + w_2(k) & x_1(k) \le 0 \end{cases} \\ x_3(k+1) = \begin{cases} \dfrac{T\beta}{V_2(x_4(k))}[-C_d w x_1(k)\sqrt{\dfrac{2}{\rho}(x_3(k))} \\ +Ax_5(k)] + x_3(k) \quad + w_3(k) & x_1(k) > 0 \\ \dfrac{T\beta}{V_2(x_4(k))}[-C_d w x_1(k)\sqrt{\dfrac{2}{\rho}(p_s - x_3(k))} \\ +Ax_5(k)] + x_3(k) + w_3(k) & x_1(k) \le 0 \end{cases} \\ x_4(k+1) = Tx_5(k) + x_4(k) + w_4(k) \\ x_5(k+1) = \dfrac{T}{m}[Ax_2(k) - Ax_3(k) - x_7(k)] + x_5(k) + + w_5(k) \\ x_6(k+1) = T[-2d_m\omega_n x_6(k) - \omega_n^2 x(k) + k_{sp}\omega_n^2 u(k+1)] \\ + x_6(k) + w_6(k) \\ x_7(k+1) = Tx_7(k) + w_7(k) \end{cases} \tag{9}$$

T represents the sampling time. Given Eq. 9, the EKF estimator is now formulated in two stages:

Stage one: time update equations (prediction):

$$\begin{cases} \hat{\boldsymbol{x}}_k^- = \mathbf{f}(\hat{\boldsymbol{x}}_{k-1}^+, u_k) \\ \mathbf{P}_k^- = \mathbf{A}_k\mathbf{P}_{k-1}^+\mathbf{A}_k^T + \mathbf{W}_k\mathbf{Q}_{k-1}\mathbf{W}_k^T \end{cases} \tag{10}$$

Stage two: measurement update equations (correction):

$$\begin{cases} \mathbf{K}_k = \mathbf{P}_k^-\mathbf{H}_k^T(\mathbf{H}_k\mathbf{P}_k^-\mathbf{H}_k^T + \mathbf{V}_k\mathbf{R}_k\mathbf{V}_k^T)^{-1} \\ \hat{\boldsymbol{x}}_k^+ = \hat{\boldsymbol{x}}_k^- + \mathbf{K}_k(\boldsymbol{y}_k - \mathbf{h}(\hat{\boldsymbol{x}}_k^-, \mathbf{0})) \\ \mathbf{P}_k^+ = (\mathbf{I} - \mathbf{K}_k\mathbf{H}_k)\mathbf{P}_k^- \end{cases} \tag{11}$$

$\hat{\boldsymbol{x}}_k^-$ and $\hat{\boldsymbol{x}}_k^+$ are the *a priori* and the *a posteriori* estimates of the system state vector, $\boldsymbol{x}_k$, respectively. $\mathbf{K}_k$ is known as the Kalman gain. $\mathbf{P}_k$, $\mathbf{Q}_k$ and $\mathbf{R}_k$ are the covariance matrices related to the state vector, $\boldsymbol{x}_k$, process noise vector, $\boldsymbol{w}_k$, and measurement noise vector, $\boldsymbol{v}_k$, respectively. $\mathbf{A}_k$, $\mathbf{H}_k$, $\mathbf{W}_k$, and $\mathbf{V}_k$ are the Jacobian matrices, elements of which are updated at each sampling time according to the following equations:

$$\mathrm{A}_{k[i,j]} = \left.\frac{\partial f_{[i]}}{\partial x_{[j]}}\right|_{(\hat{x}_{k-1}^+, u_k, 0)}$$

$$\mathrm{H}_{k[i,j]} = \left.\frac{\partial h_{[i]}}{\partial x_{[j]}}\right|_{(\hat{x}_k^-, 0)} \tag{12}$$

$$\mathrm{W}_{k[i,j]} = \left.\frac{\partial f_{[i]}}{\partial w_{[j]}}\right|_{(\hat{x}_{k-1}^+, u_k, 0)} \tag{12}$$

$$\mathrm{V}_{k[i,j]} = \left.\frac{\partial h_{[i]}}{\partial v_{[j]}}\right|_{(\hat{x}_k^-, 0)}$$

For the system under consideration, elements of matrix $\mathbf{A}_k$ are obtained as follows:

$$\mathbf{A}_k = \frac{\partial \mathbf{f}}{\partial \mathrm{x}_k} = [\frac{\partial f_1}{\partial \mathrm{x}_k}, \frac{\partial f_2}{\partial \mathrm{x}_k}, \frac{\partial f_3}{\partial \mathrm{x}_k}, \frac{\partial f_4}{\partial \mathrm{x}_k}, \frac{\partial f_5}{\partial \mathrm{x}_k}, \frac{\partial f_6}{\partial \mathrm{x}_k}, \frac{\partial f_7}{\partial \mathrm{x}_k}]^T \tag{13}$$

where

$$\frac{\partial f_1}{\partial \boldsymbol{x}_k} = [1, \quad 0, \quad 0, \quad 0, \quad 0, \quad T, \quad 0]$$

$$\frac{\partial f_2}{\partial \boldsymbol{x}_k} = \begin{bmatrix} \dfrac{T\beta}{V_1(x_4(k))}C_d w x_1(k)\sqrt{\dfrac{2}{\rho}(p_s - x_2(k))}\ , \\ 1 + \dfrac{T\beta}{V_1(x_4(k))}C_d w x_1(k)(\dfrac{-1}{\rho\sqrt{\dfrac{2}{\rho}(p_s - x_2(k))}}), \\ 0, \\ -\dfrac{T\beta}{V_1^2(x_4(k))}\dot{V}_1(x_4(k))[C_d w x_1(k)\sqrt{\dfrac{2}{\rho}(p_s - x_2(k))} \\ -Ax_5(k)], \\ \dfrac{T\beta}{V_1(x_4(k))}(-A)\ , 0\ ,\ 0 \end{bmatrix}$$

$$(x_1(k) > 0)$$

$$\frac{\partial f_2}{\partial \boldsymbol{x}_k}=\begin{bmatrix} \frac{T\beta}{V_1(x_4(k))}C_d w x_1(k)\sqrt{\frac{2}{\rho}(x_2(k))}, \\ 1+\frac{T\beta}{V_1(x_4(k))}C_d w x_1(k)(\frac{1}{\rho\sqrt{\frac{2}{\rho}(x_2(k))}}), \\ 0, \\ -\frac{T\beta}{V_1^2(x_4(k))}\dot{V}_1(x_4(k))[C_d w x_1(k)\sqrt{\frac{2}{\rho}(x_2(k))} \\ -Ax_5(k)],\ \frac{T\beta}{V_1(x_4(k))}(-A), \\ 0,\ 0 \end{bmatrix}$$

$$(x_1(k)\le 0)$$

$$\frac{\partial f_3}{\partial \boldsymbol{x}_k}=\begin{bmatrix} \frac{T\beta}{V_2(x_4(k))}\left[-C_d w x_1(k)\sqrt{\frac{2}{\rho}(x_3(k))}\right], \\ 0, \\ 1+\frac{T\beta}{V_2(x_4(k))}\left[-C_d w x_1(k)(\frac{-1}{\rho\sqrt{\frac{2}{\rho}(x_3(k))}})\right], \\ -\frac{T\beta}{V_2^2(x_4(k))}\dot{V}_2(x_4(k))[-C_d w x_1(k)\sqrt{\frac{2}{\rho}(x_3(k))} \\ +Ax_5(k)],\ \frac{T\beta}{V_2(x_4(k))}A, \\ 0,\ 0 \end{bmatrix}$$

$$(x_1(k)>0)$$

$$\frac{\partial f_3}{\partial \boldsymbol{x}_k}=\begin{bmatrix} \frac{T\beta}{V_2(x_4(k))}\left[-C_d w x_1(k)\sqrt{\frac{2}{\rho}(p_s-x_3(k))}\right], \\ 0, \\ 1+\frac{T\beta}{V_2(x_4(k))}\left[-C_d w x_1(k)(\frac{-1}{\rho\sqrt{\frac{2}{\rho}(p_s-x_3(k))}})\right], \\ -\frac{T\beta}{V_2^2(x_4(k))}\dot{V}_2(x_4(k))[-C_d w x_1(k)\sqrt{\frac{2}{\rho}(p_s-x_3(k))} \\ +Ax_5(k)],\ \frac{T\beta}{V_2(x_4(k))}A, \\ 0,\ 0 \end{bmatrix}$$

$$(x_1(k)\le 0)$$

$$\frac{\partial f_4}{\partial \boldsymbol{x}_k}=[0,\ 0,\ 0,\ 1,\ T,\ 0,\ 0]$$

$$\frac{\partial f_5}{\partial \boldsymbol{x}_k}=[0,\ \frac{T}{m}A,\ -\frac{T}{m}A,\ 0,\ 1,\ 0,\ -\frac{T}{m}]$$

$$\frac{\partial f_6}{\partial \boldsymbol{x}_k}=[-\omega_n^2 T,\ 0,\ 0,\ 0,\ 0,\ (-2d_m\omega_n T+1),\ 0]$$

$$\frac{\partial f_7}{\partial \boldsymbol{x}_k}=[0,\ 0,\ 0,\ 0,\ 0,\ 0,\ 1]$$

The EKF model generates a sequence of estimated state vector, $\hat{\boldsymbol{x}}_k^+$ given the measurements, y_k at each sampling time T. Choosing the measurements as $\mathbf{y}_k = [x_a(k), p_1(k), p_2(k)]^T$, the elements of matrix $\mathbf{H}_k$ are defined as:

$$\mathbf{H}_k=\begin{bmatrix} 0 & 0 & 0 & 1 & 0 & 0 & 0 \\ 0 & 1 & 0 & 0 & 0 & 0 & 0 \\ 0 & 0 & 1 & 0 & 0 & 0 & 0 \end{bmatrix} \tag{14}$$

Covariance matrices $\mathbf{Q}_k$ and $\mathbf{R}_k$ are considered constants assuming noises are stationary, white and Gaussian. Further, it is assumed that the noise characteristics of different system state variables are independent of each other. Thus, both $\mathbf{Q}_k$ and $\mathbf{R}_k$ are diagonal, and the values of their elements are chosen prior to the experiment based on the system response (see Section 3). The bigger this variance is, the better time-varying parameters are tracked; however, constant parameters may become noisier (Beineke et al., 1997). Finally, assuming noises are independent of each other, $\mathbf{W}_k$ and $\mathbf{V}_k$ are chosen as unity matrices.

3.3 FDI Scheme

The configuration of the FDI scheme is shown in Fig. 3. The measurements of ram displacement, x_a, and the chamber pressures, p_1 and p_2, along with the control signal, u, are used as inputs to the EKF. The two chamber pressures and actuator displacement, determined by the EKF, are then compared with actual measurements to compute the state estimation error vector, $\boldsymbol{e}_k$. Under normal operating condition the EKF model must closely predict the actual system states. Therefore, the residual error vector, $\boldsymbol{e}_k$, must stay relatively low, reflecting only the estimation errors due to modeling uncertainties. However, when actuator leakage faults occur (internal or external), the characteristic of the system changes. Theoretically, discrepancy lies between the faulty system model and the EKF model that is designed based on the normal (healthy) condition. Due to this discrepancy, the state estimation of the EKF diverges from the actual state trajectory. By observing the variation of the moving average and patterns of the residual errors, pertaining to chamber pressures only, leakage fault types and levels can be identified. Note that the EKF-based FDI scheme proposed in this paper does not include models of leakage faults as they are difficult to obtain in practice.

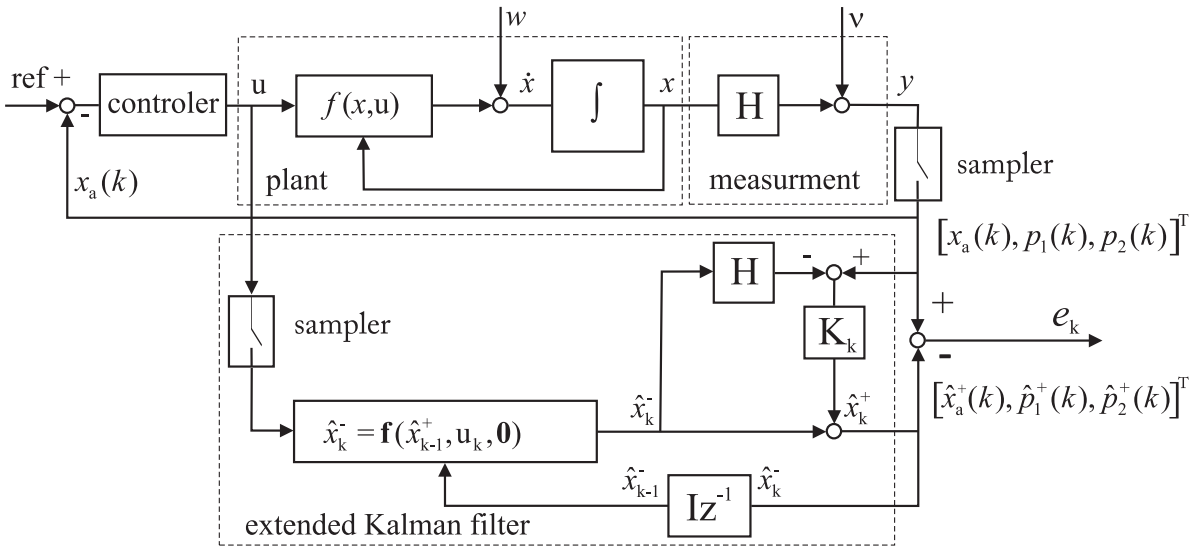

Fig. 3: *Leakage fault identification scheme*

4 Experimental Results

4.1 Description of Experiments and Tuning

Experiments are conducted using two types of reference signals for actuator displacement: sinusoidal signal and pseudorandom signal. The sinusoidal reference signal is characterized with amplitude of 0.02 m and period of 2 seconds. This signal is very structured and is ideally used for fault detection using off-line series of tests. The pseudorandom reference signal is employed to investigate the performance of the FDI scheme towards on-line applications whereby the magnitude and duration of the input signal can change. The pseudorandom signal is characterized with a series of desired step inputs having amplitudes between 0.174 m to 0.184 m and durations between 0.2 s to 4 s. This type of signal resembles activities of flaps for typical in-flight maneuvers (see for example the report by Nguyen et al., 1979), and thus allows us to investigate fault detection ability of our method utilizing on-line information. The duration for each test is 60 seconds. A high gain proportional controller is used to close the position control loop.

The parameters of the experimental test rig, used in the EKF FDI scheme, are summarized in Table 1. Parameters were obtained either directly from manufacturer's data or by careful experimental measurement, and comparisons between the results of nonlinear simulations and experimental trials. The parameters obtained in Table 1 allowed simulation results that matched the experimental results with average 2.8×10^{-4} m actuator displacement error, and average 1.45×10^{5} Pa error in line pressures. When the EKF is considered, these errors are classified as modeling uncertainties. The environment is represented by a spring having elasticity of $K_{spring} = 6.0 \times 10^{5}$ N/m.

Table 1: System parameters

A (m^2)	633×10^{-6}
m (kg)	10.0
w (m^2/m)	20.75×10^{-3}
C_d	2.915×10^{-2}
k_{sp}(V/m)	27.94×10^{-6}
ω_n (rad/s)	200π
d_m	0.7
V_1^0 , V_2^0 (m^3)	21.4×10^{-6}
p_s(Pa)	13.79×106
β (Pa)	689×106
ρ (kg/m3)	847.15

In each experiment, the initial values of the state estimates, $\hat{\boldsymbol{x}}_0^+$ were set to zeros except for the line pressures which were set to half of the pump pressure, i.e., $\hat{\boldsymbol{x}}_0^+ = [0, 6.8\times10^6, 6.8\times10^6, 0, 0, 0, 0]^T$ (units are consistent with the ones in Table 1). The initial covariance matrix, $\mathbf{P}_0^+$, was set to a sufficiently positive-definite matrix that is diagonally salient (Haykin, 2001), i.e., $\mathbf{P}_{0[i,i]}^+ = 10^4$. The covariance matrices, **Q** and **R,** were selected to produce a good convergence rate for the system under the normal operating condition and based on the combination of system noise analysis and modeling uncertainties. Initial values were selected bases on the errors between the simulation and the experimental results as outlined earlier. Further tuning was conducted by trial-and-error using a sinusoidal input signal, and observing the results of the EKF during normal operations. Matrix **Q** was finally chosen as $\mathbf{Q} = diag[10^{-20}\ \ 10^4\ \ 10^4\ \ 10^{-6}\ \ 10^{-4}\ \ 10^{-20}\ \ 10^2]$, and matrix **R** was chosen as $\mathbf{R} = diag\begin{bmatrix}10^{-4} & 10^5 & 10^5\end{bmatrix}$. Given the above parameter settings, experiments on external and internal leakages were carried out.

For every test, the system started under normal operat-

ing condition; a specific fault was then manually introduced at $t \approx 20$ s. The external leakage on either side of the actuator cylinder as well as the internal leakage between the two cylinder chambers were introduced by opening needle valves mounted on corresponding bypasses (as described earlier). Residual errors without fault (0 ~ 20 s) were compared with the ones with fault (20 ~ 60 s).

In our experiments, the sampling frequency was 1000 Hz. This frequency has been tested to be the lowest applicable sampling frequency for the EKF to effectively converge. The measurements required for each test are the actuator displacement and the cylinder pressures.

4.2 Leakage Fault Detection using Sinusoidal Input Reference signal

The first experiment relates to identification of external leakage fault as applied to chamber 1 of the actuator. The results are shown in Fig. 4 to 7. Figure 4 shows the leakage flow of average 0.32 L/min, which was introduced at t = 20 s. Given pressure differential of 12 MPa, this flow rate relates roughly to a seal opening of 0.17 mm, which is reasonable. The desired displacement (reference signal) trajectory and the actual displacement response are also shown in Fig. 4. Figures 5 and 6 show the measured (M), estimated (E) and variation of the moving average of the residual error (MAE) of individual chamber pressure when a leakage fault was introduced in chamber 1 (as shown in Fig. 4).

The moving average of the error was calculated from $\mathrm{MAE} = \frac{\sum_{i=k-n}^{k} |e_i|}{n}$, where the size of the data, n, for calculating the moving average was 4000. From Fig. 5 and 6, it is seen that with the introduction of leakage fault in chamber 1, the moving average of residual error of chamber 1 pressure increased, while the residual error of pressure at chamber 2 remained unchanged.

The external force, F_e, estimated by the EKF is shown in Fig. 7. The measured environmental force obtained from the force sensor is also given. The actuator friction was also determined by subtracting the measured environmental force from the estimation of the external force by the EKF model. With reference to Fig. 7, the value of friction force varies within [-1000, 2000 N].

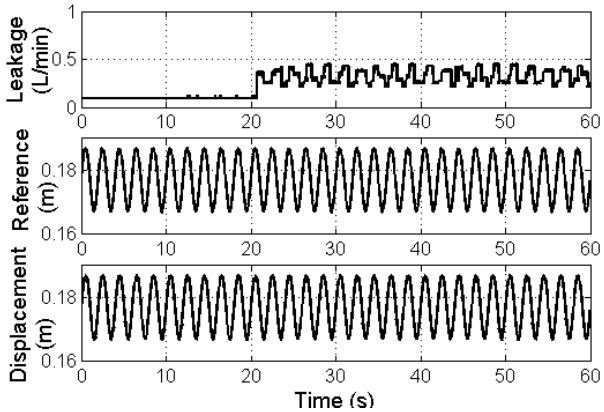

Fig. 4: *Leakage fault at chamber 1, reference (desired) actuator displacement, and measured actuator displacement (experiment 1)*

Similar results were observed when leakage was introduced in chamber 2 of the actuator, i.e., the moving average of the residual error for the pressure at chamber 2 changed within a short period of time after the introduction of leakage in the corresponding chamber. However, the moving average of the residual pressure error at chamber 1 did not change significantly after the fault.

The next test was to observe the response of the EKF-based fault detector to the internal leakage fault. This leakage was introduced by adjusting the needle valve mounted on the bypass that connects the two chambers of the actuator (see Fig. 2). Figure 8 shows the plots of the internal leakage, and the moving average of residual error of both chamber pressures.

Note that the flowmeter is indifferent to the direction of the flow; thus, only positive flow readings can be obtained in the experiments for internal leakage.

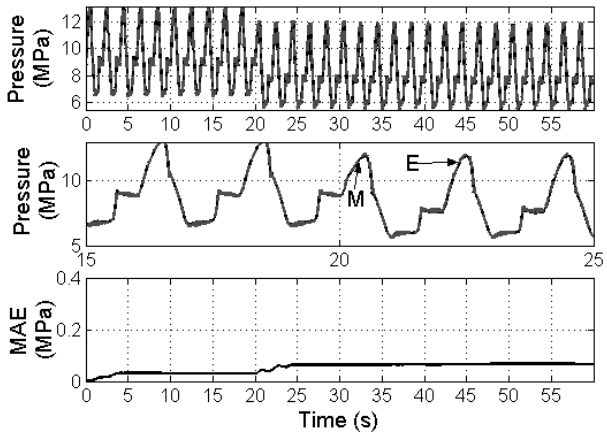

Fig. 5: *Measured (**M**) and estimated (**E**) line pressures at chamber 1; close-up plot of pressures and moving average error (**MAE**) between the measured and estimated pressures (experiment 1). Leakage fault was introduced at time t = 20 s*

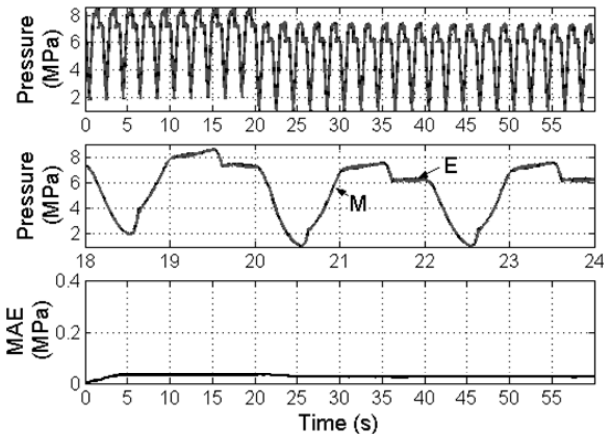

Fig. 6: *Measured (**M**) and estimated (**E**) line pressures at chamber 2; close-up plot of pressures and moving average error (**MAE**) between the measured and estimated pressures*

It can also be observed that the leakage is much higher when the actuator extends than when it retracts. The resistance due to loading plays a main role on this asymmetry. Exploring the experimental results shown in Fig. 8, it is observed that the moving average of the

residual errors of both chamber pressures increased with the introduction of an internal leakage fault.

The last experiment was to investigate whether different levels of leakage faults can be distinguished. Figures 9 to 11 show the results of implementing three types of leakage faults. Table 2 summarizes the experimental results with the emphasis on the sensitivity of the fault detector.

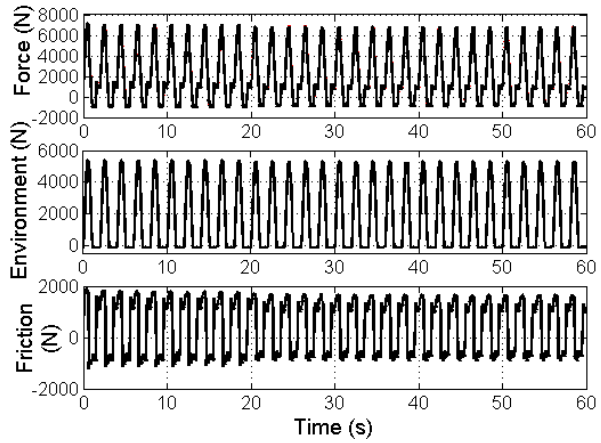

Fig. 7: *Estimated external force (environment plus friction) by the EKF, measured environmental force by the force sensor, and estimated effective actuator friction obtained by subtracting the measured environmental force from the estimated external force (experiment 1)*

The above tests clearly show that by observing the patterns of the residual errors of the chamber pressures, one could identify various leakage faults. The increase of the moving average error of one chamber only, indicates the occurrence of the external leakage in that chamber. However, when the cross-port leakage fault occurs, the moving average of residual errors for both the chamber pressures increases. These results are consistent with the observation reported in our previous work (An and Sepehri, 2005), but relate to a more practical case of actuators experiencing substantial unknown external loading and friction. In the next section, the performance of the fault detector will be examined for cases where the reference signal is unstructured.

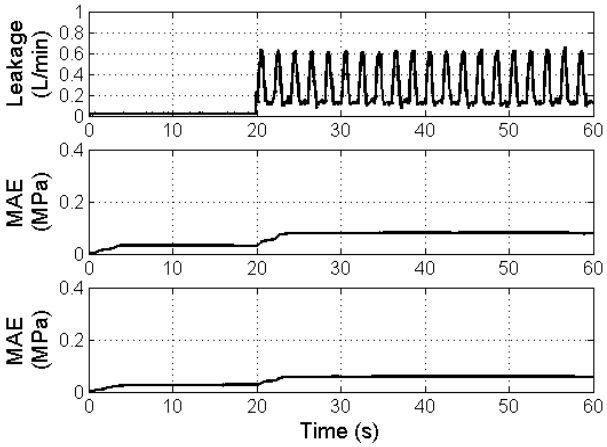

Fig. 8: *Internal leakage fault introduced at t ≈ 20 s, and the moving average error of line pressures 1 and 2 (experiment 2)*

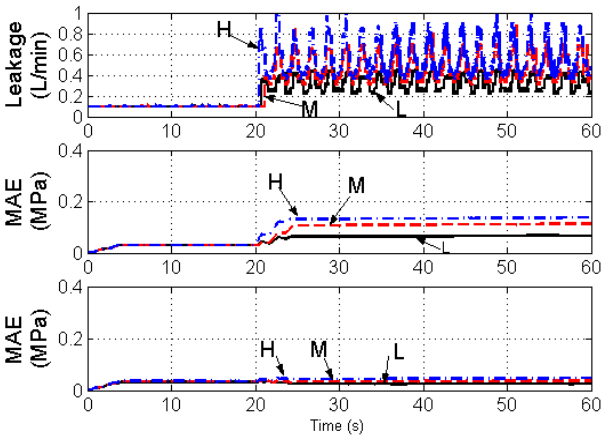

Fig. 9: *Response of fault detector to different external leakage fault levels in chamber 1 (Low, L, medium, M, and high, H). Moving average of residual pressure error in chamber 1 changes with fault level, while remains steady for chamber 2*

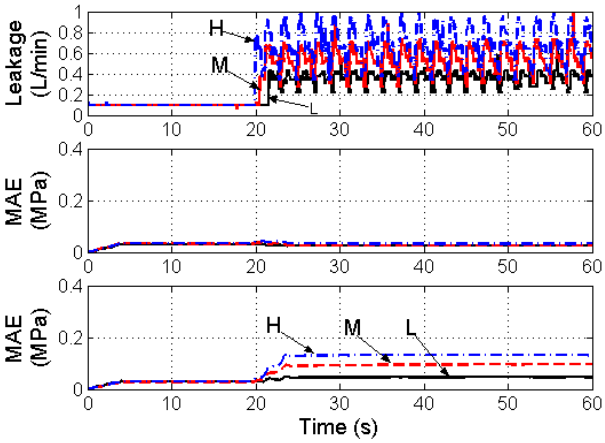

Fig. 10: *Response of fault detector to different external leakage fault levels in chamber 2 (Low, L, medium, M, and high, H). Moving average of residual pressure error in chamber 2 changes with fault level, while remains steady for chamber 1*

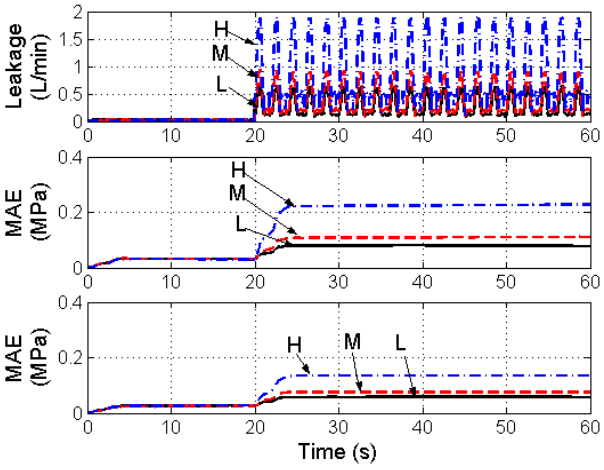

Fig. 11: *Response of fault detector to different internal leakage fault levels (Low, L, medium, M, and high, H). Moving average of residual pressure errors of both chambers change with fault levels*

Table 2: Sensitivity of fault detector to leakage fault types and levels

Leakage level	No leak	low	medium	high
Average Chamber 1 leakage (L/min)	0.09	0.32	0.46	0.56
Average residual pressure error of chamber 1 ($\times 10^5$ Pa)	0.30	0.65	1.08	1.33
Average residual pressure error of chamber 2 ($\times 10^5$ Pa)	0.34	0.25	0.35	0.45
Average Chamber 2 leakage (L/min)	0.09	0.35	0.53	0.68
Average residual pressure error of chamber 1 ($\times 10^5$ Pa)	0.32	0.26	0.26	0.34
Average residual pressure error of chamber 2 ($\times 10^5$ Pa)	0.30	0.46	0.93	1.31
Average Internal leakage (L/min)	0.02	0.26	0.38	0.84
Average residual pressure error of chamber 1 ($\times 10^5$ Pa)	0.31	0.79	1.08	2.23
Average residual pressure error of chamber 2 ($\times 10^5$ Pa)	0.26	0.58	0.75	1.34

4.3 Leakage Fault Detection using Pseudorandom Input Reference Signal

The pseudorandom position reference signal was given having randomly varying magnitude between 0.174 m to 0.184 m and duration between 0.2 s to 4 s (see Fig. 12). The test results for different levels of leakages for chambers 1 and 2, as well as the internal leakage fault, are shown in Fig. 13 to 15. The variations of the moving average of the residual errors of both chamber pressures are also shown in these figures. As is seen, the changes in the average of residual errors, in the presence of faults, are not as smooth as the ones pertaining to the sinusoidal reference signal experiments. Nevertheless, similar conclusion can be obtained.

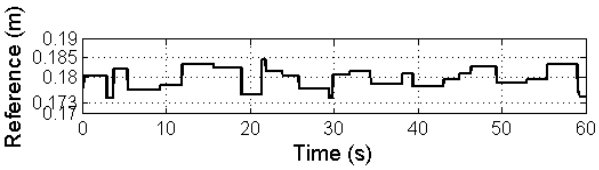

Fig. 12: *Typical pseudorandom reference position signal*

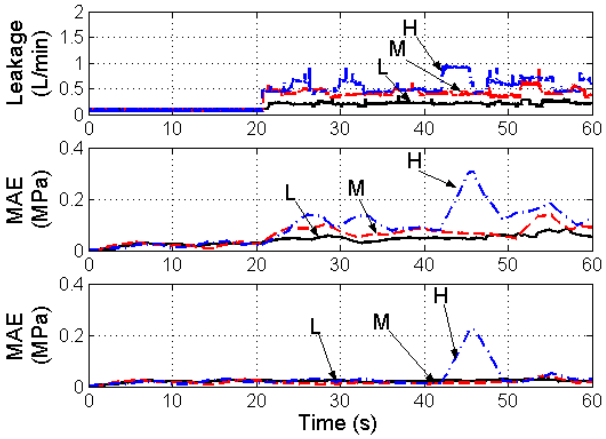

Fig. 13: *Response of fault detector to different leakage levels in chamber 1 (Low, L, medium, M, and high, H) and under pseudorandom input reference signal*

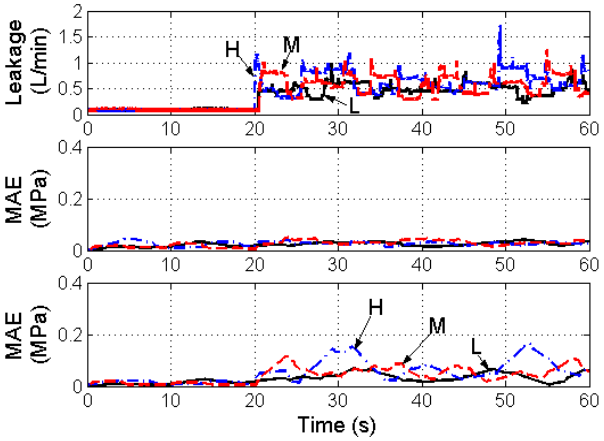

Fig. 14: *Response of fault detector to different leakage levels in chamber 2 (Low, L, medium, M, and high, H) and under pseudorandom input reference signal*

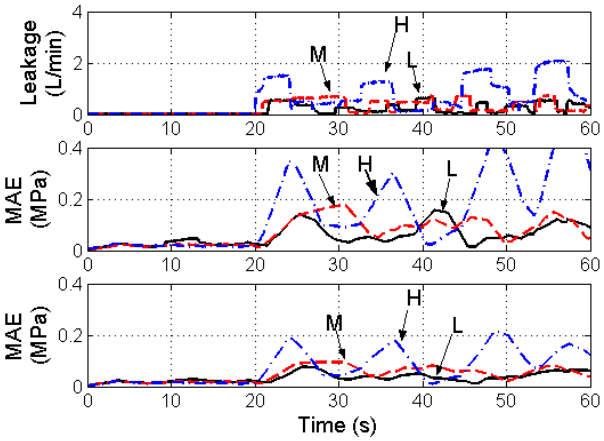

Fig. 15: *Response of fault detector to different internal leakage levels (Low, L, medium, M, and high, H) and under pseudorandom input reference signal*

By observing the changes in the residual errors of chamber pressures one could still identify the occurrence of various leakage faults in the presence of varying unknown loads. The increase in the residual error of

ing unknown loads. The increase in the residual error of one of the chambers only indicates the occurrence of the external leakage in that chamber, while the increase of the residual errors for both the chamber pressures indicates the occurrence of cross-port leakage. It was also evident that the moving average of residual errors increases proportionally with the leakage levels.

5 Conclusions

This paper presented an EKF-based fault diagnosis technique to detect various leakage faults in hydraulic actuators. The proposed scheme is an improvement over the one previously developed by the authors in that it aims at online fault detection by considering unstructured reference input signals, realistic unknown loading conditions and unmodeled actuator friction. It was experimentally shown that with three measurements, i.e., the actuator displacement and the two chamber pressures, the fault detector could identify external and internal leakage fault types and levels for actuators that are also subject to external disturbance, emulated by a strong coil spring. Given the parameter settings for the proposed FDI scheme, experiments on external and internal leakages showed that leakages as low as 0.25 L/min can be detected. Additionally, it was shown that under normal working mode, the external load, including the friction, can be reasonably estimated by the scheme. The results presented in this work, which is believed to be a contribution to the field, have thus laid a foundation for future research on developing on-line health monitoring of hydraulic actuators. Future work will take into account uncertain dynamics, drift and theoretical study of observability. Future work will also involve combining the resulting diagnostic tool and merging it with control reconfiguration (Karpenko and Sepehri, 2003) in real-time to obtain a fault-tolerant controller for hydraulic actuators that are subject to leakage faults. Presently, the algorithm runs at 1000 Hz. Combining it with a fault-tolerant controller in real-time may demand a faster computation facility.

Acknowledgments

The authors would like to thank Natural Sciences and Engineering Research Council (NSERC) of Canada for providing financial support for this research. The authors also offer their sincere thanks to the anonymous reviewers whose constructive criticisms and invaluable suggestions not only improved the quality of this paper, but also provided valuable insight into the future directions of our research in this area.

Nomenclature

C_d	Orifice coefficient of discharge	
q_1	Flow into and out of cylinder chambers 1 and 2, respectively	[m^3/s]
q_1	Flow into and out of cylinder chambers 1 and 2, respectively	[m^3/s]
w	Orifice area gradient	[m^2/m]
x_{sp}	Servo valve spool displacement	[m]
ρ	Density of hydraulic oil	[kg/m^3]
p_s	Pump pressure	[Pa]
p_1	Pressure at cylinder chambers 1 and 2, respectively	[Pa]
p_2	Pressure at cylinder chambers 1 and 2, respectively	[Pa]
x_a	Actuator displacement	[m]
A	Piston area	[m^2]
β	Effective bulk modulus	[Pa]
V_1	Volume of the fluid trapped in cylinder chambers 1 and 2, respectively	[m^3]
V_2	Volume of the fluid trapped in cylinder chambers 1 and 2, respectively	[m^3]
V_1^0	Volume of the fluid trapped in supply pipes connecting cylinder chambers 1 and 2, respectively	[m^3]
V_2^0	Volume of the fluid trapped in supply pipes connecting cylinder chambers 1 and 2, respectively	[m^3]
X_{min}	Position of the actuator when fully retracted or extended, respectively	[m]
X_{max}	Position of the actuator when fully retracted or extended, respectively	[m]
u	Valve input voltage	[V]
K_{sp}	DC gain of servo valve model	[m/V]
ω_n	Natural frequency of servo valve model	[rad/s]
d_m	Damping ratio of servo valve model	[Ns/m]
F_e	External force	[N]
K_{spring}	Young's modulus of the loading spring	[N/m]
m	Mass of ram	[kg]
$\boldsymbol{x}$	System state vector	
$\mathbf{x}_k$	Discrete system state vector	
$\boldsymbol{y}$	Output vector	
$\mathbf{A}$	Transition matrix	
$\mathbf{W}$	Process noise matrix	
$\boldsymbol{w}$	Process noise vector	
$\mathbf{H}$	Measurement matrix	
$\boldsymbol{v}$	Measurement noise vector	
$\mathbf{Q}$	Covariance matrix of process noise	
$\mathbf{R}$	Covariance matrix of measurement noise	
$\mathbf{P}_k$	Covariance matrix of transition matrix	
$\mathbf{P}_k^-$	*a priori* covariance matrix of transition matrix at discrete moment k	
$\mathbf{P}_k^+$	*a posteriori* covariance matrix of transition matrix at discrete moment k	
$\mathbf{Z}_k$	Measurement at discrete moment k	
$\hat{\mathbf{x}}_k^-$	*a priori* estimation of state vector at discrete moment k	
$\hat{\mathbf{x}}_k^+$	*a posteriori* estimation of state vector at discrete moment k	

$\mathbf{K}_k$	Kalman gain matrix at discrete moment k	
$\mathbf{P}_0^+$	Initial covariance matrix of transition matrix	
$\hat{\mathbf{x}}_0^+$	Initial state vector	
$\boldsymbol{e}_k$	State estimation error vector	
T	Sampling period	[s]

References

An, L. and **Sepehri, N.** 2003. Hydraulic actuator circuit fault detection using extended Kalman filter. *Proceedings: American Control Conference*, pp. 4261-4266.

An, L. and **Sepehri, N.** 2005. Leakage fault identification in a hydraulic positioning system using extended Kalman filter. *International Journal of Fluid Power,* Vol. 6, pp. 41-51.

Beineke, S., **Schutte, F.** and **Grotstollen, H.** 1997. Online identification of nonlinear mechanics using extended Kalman filters with basis function networks. *Proceedings: Conference on Industrial Electronics, Control and Instrumentation*, pp. 316 -321.

Chinniah, Y., **Burton, R.** and **Habibi, S.** 2003. Viscous damping coefficient and effective bulk modulus estimation in a high performance hydrostatic system using extended Kalman filter. *International Journal of Fluid Power,* Vol. 4, pp. 27-34.

Crowther, W. J., **Edge, K. A.**, **Atkinson, R. M.** and **Woollons, D. J.** 1998. Fault diagnosis of a hydraulic actuator circuit using neural networks - an output vector space classification approach. *Proceedings: of Institution of Mechanical Engineers,* Vol. 212, pp. 57-68.

Frank, P. M 1994. On-line fault detection in uncertain nonlinear systems using diagnostic observers: a survey. *International Journal of Systems Science,* Vol. 25, pp. 2129-2154.

Haykin, S. 2001. *Kalman filtering and neural networks*. John Wiley & Sons.

Karpenko, M. and **Sepehri, N**. 2003. Robust position control of an electrohydraulic actuator with faulty actuator seal. *ASME J. of Dynamic Systems, Measurement and Control,* Vol. 125, pp. 413-423.

Khan, H., **Abou, S.** and **Sepehri, N.** 2005. Nonlinear observer-based fault detection technique for electrohydraulic servo-positioning systems. *International J. of Mechatronics,* Vol. 15, pp. 1037-1059.

Le, T. T., **Watton, J.** and **Pham, D. T.** 1998. Fault classification of fluid power systems using a dynamics feature extraction technique and neural networks. *Proceedings of the Institution of Mechanical Engineers,* Vol. 212, pp. 87-96.

Merritt, H. E. 1967. *Hydraulic Control Systems*. John Wiley & Sons.

Nguyen, L. T., **Ogburn, M. E.**, **Gilbert, W. P.**, **Kibler, K. S.**, **Brown P. W.** and **Deal, P. L.** 1979. Simulation study of stall/post-stall characteristics of a fighter airplane with relaxed static stability. *NASA Langley Research Center*, Hampton, VA, Tech. Rep. NASA-TP-1538.

Skormin, V. A., **Apone, J.** and **Dunphy, J. J.** 1994. On-line diagnostics of a self-contained flight actuator. *IEEE Transactions on Aerospace and Electronic Systems,* Vol. 30, pp. 186-196.

Skormin, V. A. and **Apone, J.** 1995. On-line diagnostics of a variable displacement pump of a flight actuation system. *Proceedings: IEEE National Aerospace and Electronics Conference*, pp. 503-510.

Zavarehi, M. K., **Lawrence, P. D.** and **Sassani, F.** 1999. Nonlinear modeling and validation of solenoid-controlled pilot-operated servovalves. *IEEE/ASME Transactions on Mechatronics,* Vol. 4, pp. 324-334.

Zhang, Y. M. and **Jiang, J.** 2002. Active fault-tolerant control system against partial actuator failures. *IEEE Proceedings of Control Theory Application,* Vol. 149, pp. 95-104.

Zhou, R., **Lin, T.**, **Han, J.** and **Yan, D.** 2002. Fault diagnosis of airplane hydraulic pump. *Proceedings: World Congress on Intelligent Control and Automation*, pp. 3150-3152.

Liang An
received B.Sc. in Automation Engineering from the Zhengzhou Institute of Technology in 1993, M.Sc. in Control Engineering from the Beijing University of Chemical Technology in 1999, Ph.D. in fluid power systems and diagnosis from the University of Manitoba in 2007. He is currently with the Can-K Artificial Lift Systems Inc., Edmonton, Canada.

Nariman Sepehri
is a professor with the Department of Mechanical and Manufacturing Engineering, at the University of Manitoba. He received M.Sc. and Ph.D. both from the University of British Columbia. His areas of interest include telerobotics applied to hydraulic manipulators and fluid power fault tolerant control and diagnosis systems.